China Geology 8 (2025) 676−690

China Geology

Journal homepage: http://chinageology.cgs.cn
https://www.sciencedirect.com/journal/china-geology

Impacts of random negative training datasets on machine learning-based geologic hazard susceptibility assessment

Hao Cheng[a], Wei Hong[b, c,*], Zhen-kai Zhang[d], Zeng-lin Hong[a, d], Zi-yao Wang[d], Yu-xuan Dong[e]

[a] *School of Earth Science and Resources, Chang'an University, Xi'an* 710064, *China*
[b] *Xi'an Center of China Geological Survey, China Geological Survey, Ministry of Natural Resources, Xi'an* 710119, *China*
[c] *College of Urban and Environmental Sciences, Northwest University, Xi'an* 710127, *China*
[d] *Natural Resources Shaanxi Satellite Application Technology Center, Xi'an* 710119, *China*
[e] *School of Foreign Studies, China University of Petroleum (East China), Qingdao* 266580, *China*

ARTICLE INFO

Article history:
Received 25 May 2024
Received in revised form 5 November 2024
Accepted 8 November 2024
Available online 15 November 2024

Keywords:
Landslides
Debris flows
Collapses
Ground fissures
Geologic hazard prevention and control engineering
Geologic hazard susceptibility assessment
Negative training dataset
Average spatial correlation
Random forest algorithm
Risk and *return* analysis
Geological survey engineering
Loess Plateau area

ABSTRACT

This study investigated the impacts of random negative training datasets (NTDs) on the uncertainty of machine learning models for geologic hazard susceptibility assessment of the Loess Plateau, northern Shaanxi Province, China. Based on randomly generated 40 NTDs, the study developed models for the geologic hazard susceptibility assessment using the random forest algorithm and evaluated their performances using the area under the receiver operating characteristic curve (AUC). Specifically, the means and standard deviations of the AUC values from all models were then utilized to assess the overall spatial correlation between the conditioning factors and the susceptibility assessment, as well as the uncertainty introduced by the NTDs. A *risk* and *return* methodology was thus employed to quantify and mitigate the uncertainty, with log odds ratios used to characterize the susceptibility assessment levels. The *risk* and *return* values were calculated based on the standard deviations and means of the log odds ratios of various locations. After the mean log odds ratios were converted into probability values, the final susceptibility map was plotted, which accounts for the uncertainty induced by random NTDs. The results indicate that the AUC values of the models ranged from 0.810 to 0.963, with an average of 0.852 and a standard deviation of 0.035, indicating encouraging prediction effects and certain uncertainty. The *risk* and *return* analysis reveals that low- *risk* and high-*return* areas suggest lower standard deviations and higher means across multiple model-derived assessments. Overall, this study introduces a new framework for quantifying the uncertainty of multiple training and evaluation models, aimed at improving their robustness and reliability. Additionally, by identifying low-*risk* and high-*return* areas, resource allocation for geologic hazard prevention and control can be optimized, thus ensuring that limited resources are directed toward the most effective prevention and control measures.

1. Introduction

Geologic hazard susceptibility assessment is critical to geologic hazard prevention (Youssef AM et al., 2023). The assessment efficiency and reliability have been improved significantly with the advancement in remote sensing (RS) and geographic information systems (GISs) (Hu Y et al., 2022) since RS-derived data and GIS spatial analysis tools are identified as fundamental components for the assessment (Giordan D et al., 2022). Empirical knowledge-based spatial modelling methods have been extensively applied to geologic hazard susceptibility assessment (Liang SY et al., 2010), including Analytical Hierarchy Process (AHP) (Abuzied SM and Mansour BMH 2019), fuzzy logic (Tazik E et al., 2014), frequency ratio (FR) (Alireza A et al., 2019), AHP combined with GIS-based statistical models (Tazik E et al. 2014), and information value models (Liu Y et al., 2018). Although empirical knowledge methods are simple and convenient, they rely heavily on the subjective judgment of experts. This might lead to a lack of objective quantitative assessment and increased risks of subjective errors, thus potentially compromising the accuracy of assessment results (Li T et al.,

First author: *E-mail address*: 2022027015@chd.edu.cn (Hao Cheng).

* Corresponding author: *E-mail address*: hao@xaufe.edu.cn (Wei Hong).

Literary editor: Li-qiong Jia
doi:10.31035/cg2024094
2096-5192/© 2025 China Geology Editorial Office.

2024).

In recent years, machine learning has been increasingly applied to geologic hazard susceptibility assessment (Yang Z et al., 2024), with primary algorithms involved including boosted regression tree (Alireza A et al. 2019), generalized linear model (He Y and Zhang Y 2022), random forest (RF), and multivariate discriminant analysis (MDA; Liu L et al., 2021). Machine learning models driven by supervised data exhibit higher prediction accuracy than those based on empirical knowledge (Chang Z et al., 2020). However, with the increasingly wide application of machine learning to geologic hazard susceptibility assessment, uncertainties arising from different combinations of data types, data attributes, and machine learning models considering geological and environmental factors have become prominent. Several studies have been conducted on this topic. Kavzoglu T et al. (2015) used a genetic algorithm for feature selection, combined with logistic regression (LR), to determine the optimal combination of landslide conditioning factors, achieving decreased uncertainty and enhanced performance of landslide susceptibility models. Huang F et al. (2021) employed the FR method, along with six different data-driven models (i.e., FR, grey relational degree, LR, multilayer perceptron, C5.0 decision tree, and RF), to investigate the effects of varying attribute intervals and different models on the uncertainty of landslide susceptibility prediction under 36 conditions. Huang F et al. (2024) examined the relationships between landslides and environmental factors, which introduce uncertainty to landslide susceptibility prediction. Zhao Z and Chen J (2023) proposed a robust discretization criterion to quantify the uncertainty and subjectivity associated with different discretization methods using both original classification datasets and optimized datasets generated with GeoDetector software. Quantifying the uncertainties of machine learning models and mitigating them remain a major challenge in developing geologic hazard susceptibility assessment models.

Regarding the impacts of NTDs on model uncertainty, supervised data-driven geologic hazard susceptibility assessment typically utilizes training datasets containing both positive training datasets and NTDs. Positive training datasets are usually derived from known geologic hazard points, while NTDs are frequently randomly generated using software (Zuo R and Wang Z 2020). The selection of NTDs can greatly affect the assessment accuracy of models, with uncertainty being introduced in the case where random NTDs are employed (Zuo R et al., 2015). Some studies have been conducted on the impacts of NTDs on model uncertainty. Chang Z et al. (2023) constructed a model for landslide susceptibility assessment by randomly selecting non-landslide points from non-landslide areas repeatedly. Using this model, they calculated landslide susceptibility indices to quantify the model uncertainty. Their findings suggest more scientifically accurate landslide susceptibility assessment. Nykanen V et al. (2015) found that the AUC varied with the NTDs used. They found that using known nickel-copper deposits as positive datasets and randomly generated NTDs from drilling sites with the absence of mineralization. Their results also indicate that using other known deposit types as NTDs resulted in higher AUC values. Gao Y et al. (2016) assessed the impacts of NTDs on the performance of a copper polymetallic mineralization model, discovering that different NTDs led to varying AUC values when they employed five sets of randomly generated points as NTDs to train the RF model. However, none of these studies quantified the model uncertainty introduced by random NTDs or proposed any theoretical framework to mitigate uncertainty.

This study innovatively proposed a framework to reduce the impacts of random NTDs on the accuracy and performance of the models for geologic hazard susceptibility assessment. Specifically, the training dataset was constructed by selecting geologic hazard points as positive training datasets and an equal number of random non-geologic hazard points as NTDs. A total of 13 susceptibility assessment factors were determined: Altitude, curvature, aspect, slope, lithology, distances from faults, rivers, roads, and settlements, normalized difference vegetation index (NDVI), land use, rainfall, and interferometric synthetic aperture radar (InSAR). Using the RF algorithm, 40 models for geologic hazard susceptibility assessment were developed based on different NTDs. Then, the mean AUC values and standard deviations of the 40 models were used to quantify the overall spatial correlations of these models with the uncertainty introduced by NTDs. Finally, statistical methods for *risk* and *return* were employed to quantify the uncertainty caused by random NTDs, and the odds ratios were used to describe the high and low geologic hazard probabilities of the assessment outcomes. *Risk* and *return* maps were plotted using the means and standard deviations of the log odds ratios of various locations. The average log odds ratios were then converted into average probabilities, which represented the final assessment results and accounted for uncertainty caused by random NTDs. This study mitigates the uncertainty of the models introduced by NTDs. It will improve the efficiency of geologic hazard prevention and control, especially in the geologic hazard-prone Loess Plateau in northern Shaanxi, China.

2. Materials and methods

2.1. Study area

The Loess Plateau in northern Shaanxi, recognized as the most representative region featuring loess deposits and landforms in China, exhibits a fragmented surface with numerous ravines, severe soil erosion, and high susceptibility to geologic hazards (Gan Z et al., 2004). This plateau extends from 34.30°N to 39.60°N and from 106.30°E to 111.50°E, covering a total area of 79490 km² (Fig. 1). Its western and southwestern parts are dominated by mountains, while the gully and valley networks are widely distributed throughout the region. The Loess Plateau exhibits altitudes ranging from 340 m to 2430 m, slopes from 0° to 80°, and curvatures from −81 m to 70 m. Contemporarily, its gully density varies from

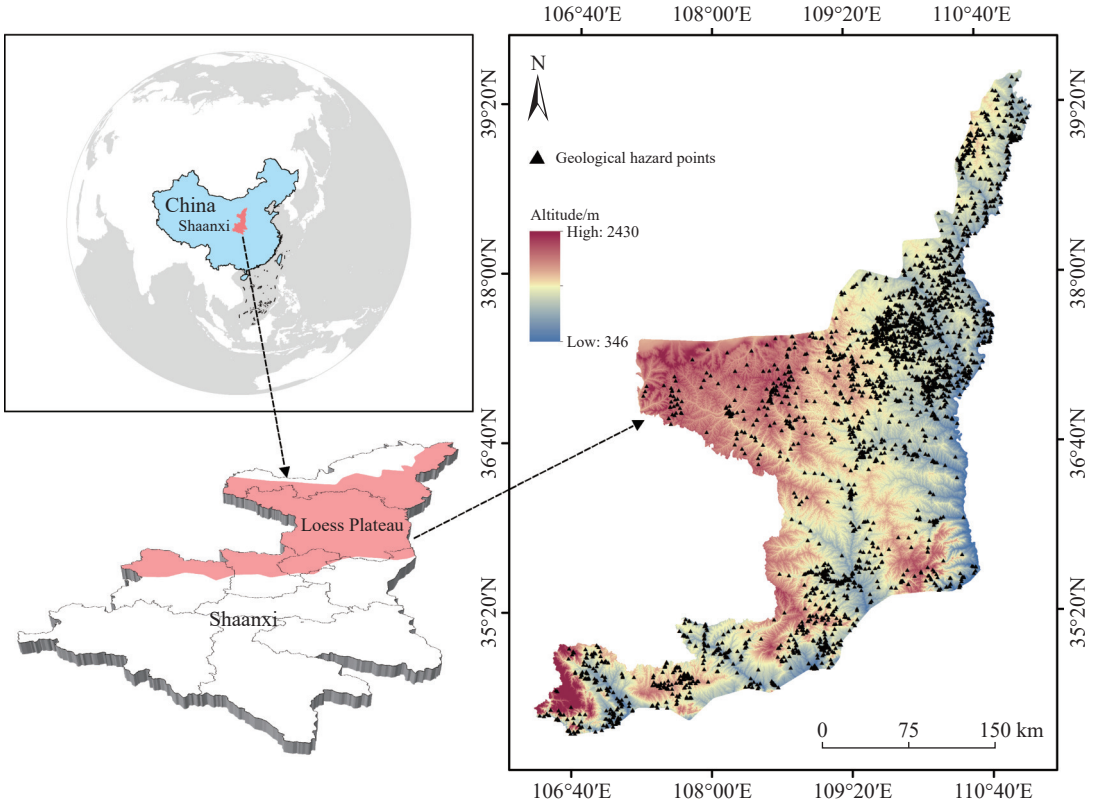

Fig. 1. Location of the Loess Plateau in northwest China.

approximately 4 km/km² to 5 km/km², with a ratio between the inter-gully and inter-ridge areas of 6∶4. It displays a surface fracture density of around 50%. The intersecting gullies lead to fragmented terrain, frequently triggering geologic hazards such as loess collapses and landslides (Matsunaga K and Gan Z 2007; Shi Q et al., 2007).

2.2. Methodology

This study aims to quantify the uncertainty of models for geologic hazard susceptibility assessment introduced by random NTDs and proposes a framework for enhancing the model accuracy and reliability using statistical optimization. First, a comprehensive analysis of the geological conditions and topography of the Loess Plateau was conducted, identifying 13 key factors influencing geologic hazards, including altitude, slope, and lithology. Then, historical geologic hazard data and environmental characteristics were employed to construct a dataset containing both positive training datasets and NTDs, which was converted into the input variables of the model. The RF algorithm was used to train the dataset, allowing the model to learn the complex relationships between input variables and geologic hazards. The RF algorithm can effectively handle multivariate data and capture nonlinear patterns, thus improving the model's prediction accuracy. The AUC values were used to evaluate the generalization ability of the model. To quantify the uncertainty introduced by random NTDs, the *risk* and *return* analysis was employed, with the log odds ratios used to characterize the susceptibility assessment levels. The *risk* and *return* values of various assessment units were calculated. Scatter plots were used to illustrate the relationship between *risk* and *return*, revealing that geological hazard points are concentrated in low-*risk*, high-*return* areas. This offers a new perspective for the risk management of geological hazards. An overview of the methodology and modeling process is illustrated in Fig. 2, highlighting the systematic study and design of a model for geologic hazard susceptibility assessment using a quantitative approach.

In sum, the entire research process can be divided into several key steps. First, data were collected and machine learning datasets were constructed while ensuring the high representativeness and generalizability of datasets. Next, the RF algorithm was used to train the dataset, producing 40 models for geologic hazard susceptibility assessment. To ensure reliable model predictions, the model accuracy was tested based on the AUC values. Using these models, the probability values of the geologic hazards were calculated and the uncertainty introduced by random NTDs was qualified using the *risk* and *return* analysis. This approach accounts for the geologic hazard susceptibility in the predictions while enhancing their overall model performance and reliability.

2.3. Data

2.3.1. Conditioning factors

Data on the historical geologic hazard events in the study area were obtained from the Department of Natural Resources of Shaanxi Province. Specifically, the data on 2850 geologic hazard events were collected, consisting of 1666 loess

collapses and 1184 loess landslides. Geologic hazards in the Loess Plateau are dominated by loess collapses and landslides due to its unique topography. Given their similarities in mechanisms and occurrence conditions, loess collapses and landslides were considered together under a unified 'collapse-landslide' model (Xu C et al., 2023). The occurrence of both geologic hazard types depends on the local geological environment of slopes, while factors such as terrain stratigraphic lithology tend to stabilize spatially. Thus, this study integrated loess collapses and landslides into a unified model for analysis (Gao R et al., 2021). Based on the mechanisms behind both geologic hazard types, this study selected 13 conditioning factors to create a feature database for model training: altitude, curvature, aspect, slope, lithology, distances from faults, rivers, roads, and settlements, NDVI, land use, rainfall, and InSAR (Meng Z et al., 2021; Zhang H et al., 2022). These conditioning factors are detailed in Table 1 and Fig. 3.

It is essential to ensure that there is no significant linear relationship between the 13 conditioning factors. Hence, this study calculated the Pearson correlation coefficients of all conditioning factors by dividing the covariance between two variables by the product of their standard deviations, as shown in Eq. 1.

$$r = \frac{\sum_{i=1}^{n}(x_i - \bar{x})(y_i - \bar{y})}{\sqrt{\sum_{i=1}^{n}(x_i - \bar{x})^2}\sqrt{\sum_{i=1}^{n}(y_i - \bar{y})^2}} \quad (1)$$

where n is the quantity of variables, x_i and y_i are the ith x and y variables, respectively. $\bar{x}$ and $\bar{y}$are the averages of x_i and y_i, respectively.

The resulting correlation coefficients range from −1 to 1. A higher absolute value of the correlation coefficient corresponds to a stronger linear correlation between the variables, except for 0, which indicates no linear dependence between the two variables (Yao J et al., 2020).

2.3.2. Preparation of training and testing datasets

Geologic hazard points were used as positive training

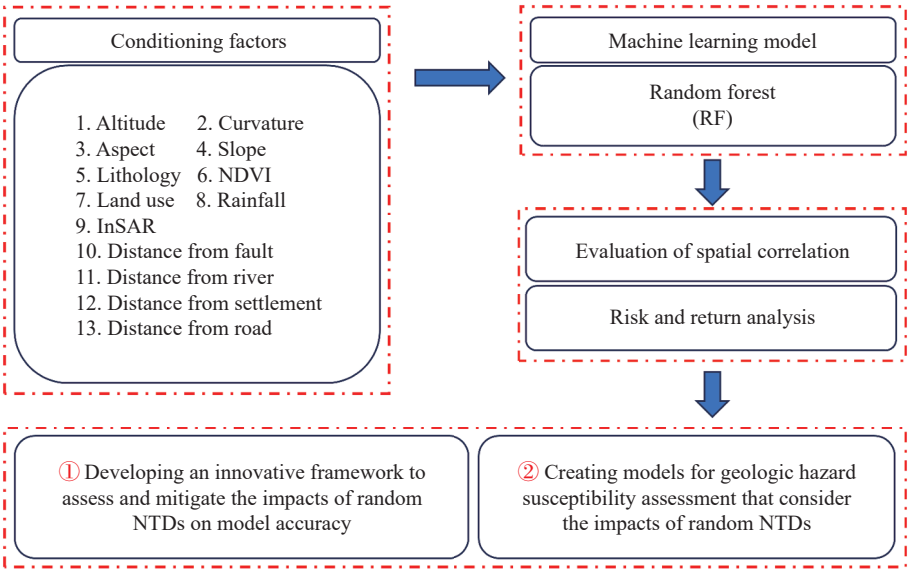

Fig. 2. Flow chart of the modelling process.

Table 1. Geologic hazard conditioning factors.

Category	Conditioning factor	Source	Data type	Spatial resolution
Terrain and landforms	Altitude	DEM	Continuous	90 × 90 m
	Curvature			
	Aspect			
	Slope			
Geotechnical conditions	Lithology	National map	Categorical	1∶100000
Geological conditions	Distance from faults	National map	Continuous	90 × 90 m
Hydrological conditions	Distance from rivers	National map	Continuous	90 × 90 m
Environmental conditions	NDVI	Official organization	Continuous	30 × 30 m
	Land use			
Human engineering activities	Distance from settlements	Official organization	Continuous	90 × 90 m
	Distance from roads			
Climate conditions	Rainfall		Continuous	90 × 90 m
Surface deformation	InSAR	Sentinel-1	Continuous	20 × 20 m

datasets, while non-geologic hazard points, generated using the ArcGIS software, constituted NTDs (Wang Q et al., 2013). A total of 40 NTDs were randomly created. The dataset consisting of these NTDs and positive training datasets was then divided into training datasets (70%) for modelling and testing datasets (30%) for assessment. Each training dataset consisted of NTDs and the positive training datasets, with the number of NTDs equal to that of the

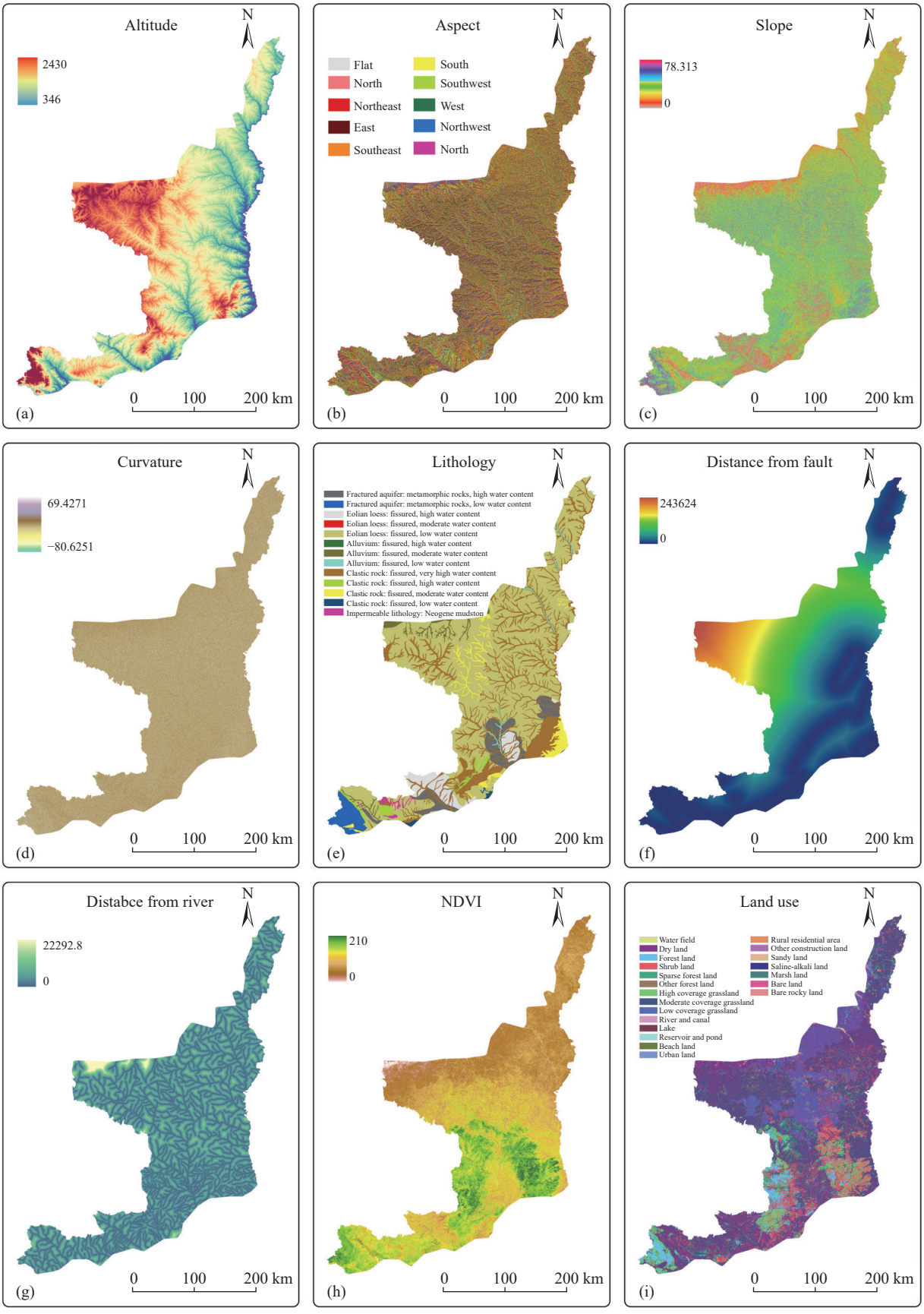

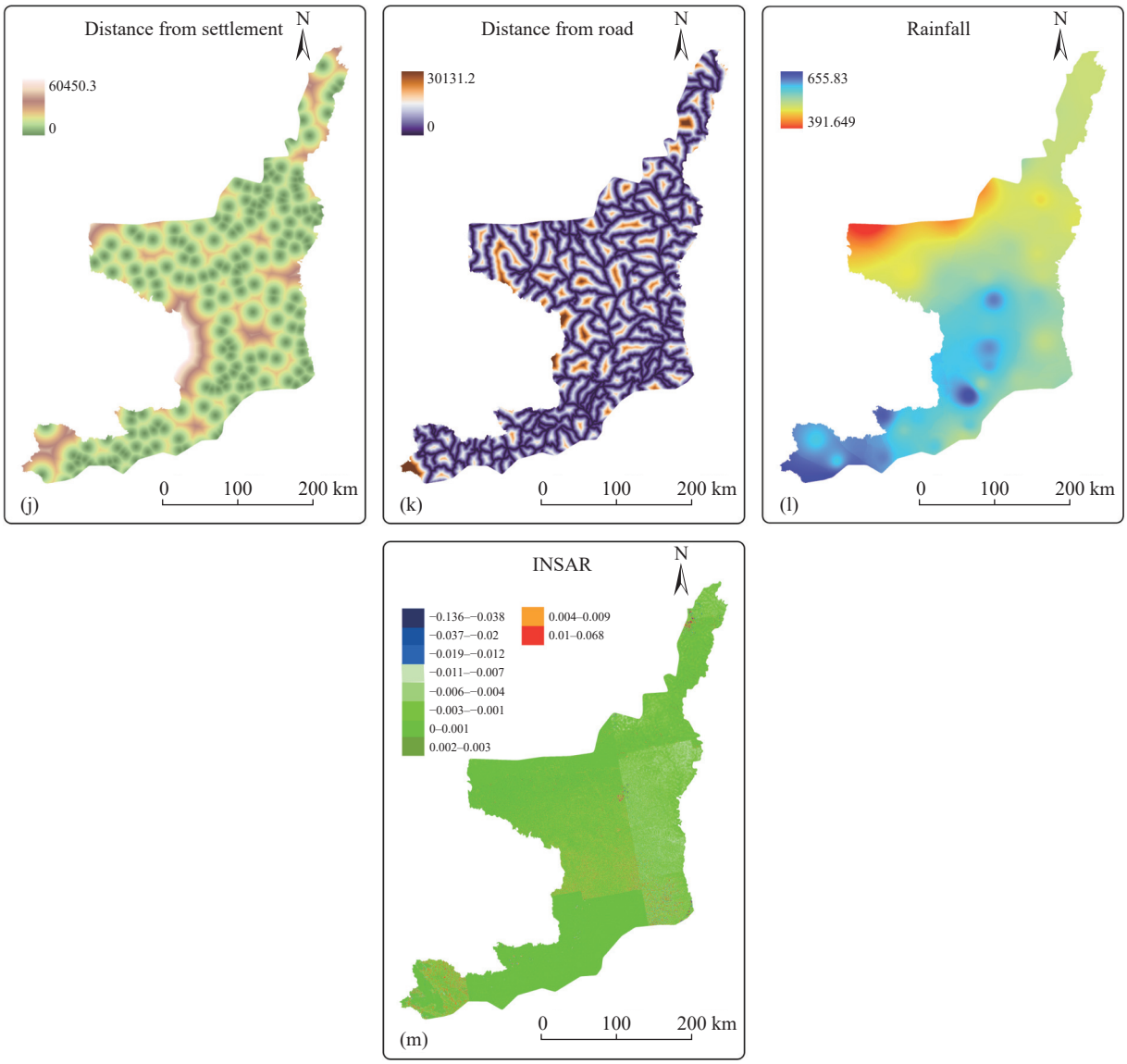

Fig. 3. Geologic hazard conditioning factors: a–Altitude; b–aspect; c–slope; d–curvature; e–lithology; f–distance from faults; g–distance from rivers; h–NDVI; i–land use; j–distance from settlements; k–distance from roads; l–rainfall; m–InSAR.

positive training datasets (Yang F et al., 2023). Fig. 4 illustrates the spatial distribution of samples in four training datasets. Both datasets were converted to the raster format with a pixel size of 90 m, where geologic hazard points and non-geologic hazard points were denoted by 1 and 0, respectively. Finally, the training dataset was overlaid with 13 conditioning factors to extract attribute values.

2.4. Evaluation of spatial correlation

RF, an ensemble algorithm based on decision trees, performs classification or regression by constructing multiple decision trees and determining the final result using a voting mechanism. This algorithm has been widely applied to geologic hazard assessment, especially the assessment of the susceptibility to collapses and landslides (Merghadi A et al., 2020). Using the RF algorithm, this study constructed models for geologic hazard susceptibility assessment based on the 13 conditioning factors. The receiver operating characteristic (ROC) curve emerges as a robust method for assessing the performance of the assessment models (Chen C et al., 2018). The ROC curve, representing the relationship between geologic hazard probability and the false positive rate, can determine the model performance under various probability thresholds using the true positive rate, false positive rates, and AUC. Among them, AUC, referring to the area under a ROC curve, can measure the degree of the correlation between a feature factor and an assessment model, along with the impacts of different NTDs on the model performance. The AUC values range from 0 to 1, with those close to 1 indicating superior performance and those approaching 0.5 suggesting suboptimal performance (Wang H et al., 2021). Finally, the means of the 40 groups of AUC values were used to measure the overall spatial correlations between the conditioning factors and the assessment models.

2.5. Risk and return analysis

This study employed a *risk* and *return* analysis model to

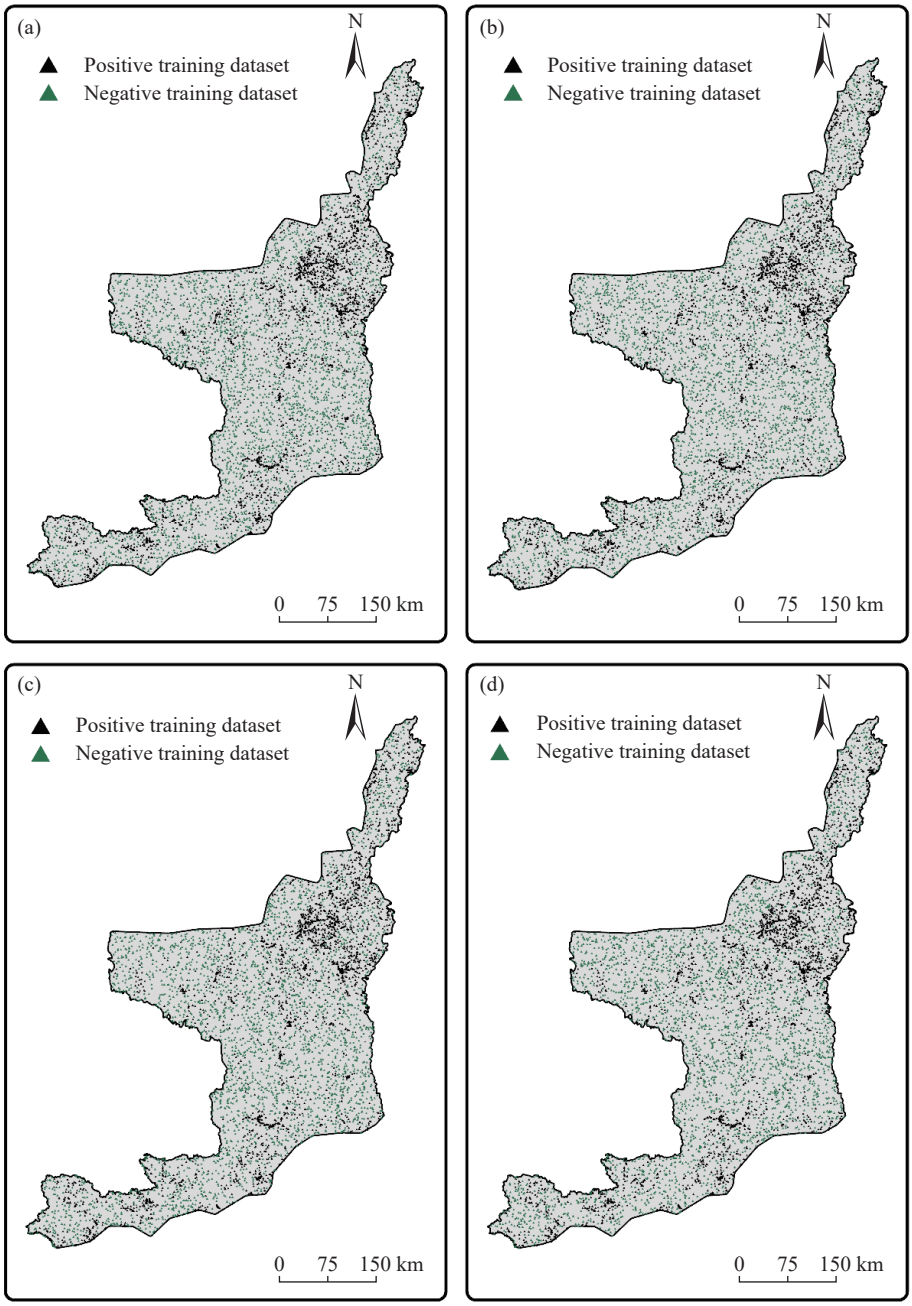

Fig. 4. Spatial distributions of positive and negative samples in randomly selected four training datasets.

quantify and mitigate the uncertainty of the geologic hazard susceptibility assessment models introduced by random NTDs (Wang Z et al., 2020; Yang F et al. 2023). In statistical analysis, *risk* generally refers to the degree of potential loss or uncertainty, while *return* represents the potential gains or benefits from decision making (Aida T and Silvia D 2014). In this study, *risk* is defined as the instability of assessment results or the potential deviation between predicted outcomes and actual occurrences. This index can be quantified by measuring the variability in the predictions induced by randomly generated NTDs. The *return* is defined as the average geologic hazard susceptibility level of the same assessment unit across multiple models, indicating the overall prediction effect of the models. High *risk* represents significant variability in the predictions of the same assessment unit across different models, suggesting low prediction reliability. In contrast, high *return* suggests the consistently high susceptibility to geologic hazards of the same assessment unit across multiple models.

Previous studies revealed cases where a prediction model yielded surprisingly low susceptibility for certain assessment units, which exhibited high geologic hazard rates in practice. This suggests the low prediction accuracy for some regions. To address this issue, this study measured the geologic hazard susceptibility of various assessment units using the log odds ratio (Camminatiello I et al., 2014; Zuo R and Wang Z 2020). Acting as a comprehensive measure for geologic hazard susceptibility, the log odds ratio refers to the natural logarithm of the ratio between the probabilities of occurrence and nonoccurrence, as shown in Eq. 2:

$$\log O(p) = \log\left(\frac{p}{1-p}\right) \tag{2}$$

where p represents the occurrence probability of geologic hazards of each assessment unit.

In this study, *risk* was calculated as the standard deviation of the log odds ratio, as shown in Eq. 3.

$$risk(X) = \frac{1}{L-1}\sum_{l=1}^{L}(\log O(p(X^{(l)})) - \overline{\log O})^2 \tag{3}$$

A higher standard deviation is associated with greater variability in the predictions, thereby reflecting increased risk. By analysing the *risk*, this study can more accurately assess the predictive performance of the models and identify the assessment units with a high actual hazard incidence but low hazard susceptibility. This will assist in making more informed decisions regarding geologic hazard risk management in these units.

In contrast, *return* was measured using the mean of the log odds ratio, as shown in Eq. 4:

$$return(X) = \overline{\log O} = \frac{1}{L}\sum_{l=1}^{L}\log O(p(X^{(l)})) \tag{4}$$

where L is the quantity of the predictive maps of geologic hazard susceptibility assessment (40 in this study), and $p(X^{(l)})$is the probability of the geologic hazard susceptibility of assessment unit X.

Therefore, *return* reflects the overall performance and reliability of model predictions. A higher mean suggests more consistently accurate model predictions. This study aims to reveal the relationship between low uncertainty and high average probability, which can be classified as 'low *risk* and high *return'* in statistics (Yhip T M and Alagheband BMD, 2020).

The log odds ratio is widely used in statistics, especially in scenarios involving binomial distributions such as the occurrence or non-occurrence of geologic hazards. Although its mean provides valuable insights into the likelihood of an event, the log odds ratio is not a direct probability. Fortunately, this ratio can be converted into a probability using Eq. 5, thus making the results more intuitive and easier to interpret.

$$P(x) = \frac{1}{[1+(e^{return(x)})]} \tag{5}$$

This equation is commonly known as a logistic function, converting the log odds ratio into a probability between 0 and 1.

3. Results

3.1. Selection of conditioning factors

The correlation matrix of the 13 conditioning factors is shown in Fig. 5. Previous studies have demonstrated that a correlation coefficient exceeding 0.7 (absolute value) indicates a high degree of collinearity between two variables (Bui D T et al., 2016). In this study, all the correlation coefficients ranged from −0.00 to 0.54, suggesting that all the conditioning factors passed correlation tests. The strongest correlation occurred between altitude and distance from faults, with a correlation coefficient of 0.54, also below the threshold of 0.7. Therefore, the 13 conditioning factors can be applied to models for geologic hazard susceptibility assessment. It is essential to interpret the correlation matrix in the context of the broader geological and environmental setting. For instance, the moderate correlation between altitude and distance from faults may reflect underlying geological processes that shape landscapes and influence geologic hazard distribution. Understanding these correlations can provide valuable insights into the spatial distribution of hazards and help improve the accuracy and reliability of the models. Overall, the correlation analysis serves as the crucial preliminary assessment to ensure that a model is developed based on independent variables, thus laying a statistically sound foundation.

3.2. Assessment of spatial correlations

To assess the spatial correlations between the 13 conditioning factors and geologic hazards in the Loess Plateau, northern Shaanxi, this study determined 40 AUC values using 40 training datasets consisting of various NTDs and positive training datasets. Fig. 6 presents the ROC curves of models constructed using the four training datasets illustrated in Fig. 4. The histogram of 40 AUC values is shown in Fig. 7, indicating that models constructed using various NTDs yielded different AUC values. The AUC values ranged from 0.810 to 0.963, with an average of 0.852 and a standard deviation of 0.035. Since all AUC values exceeded 0.5, there existed strong spatial correlations between the index system comprising the 13 conditioning factors and geologic hazards in the Loess Plateau. The variations in the AUC values indicate that the randomly selected NTDs influences the spatial correlations between conditioning factors and geologic hazards. The average AUC value of 0.852 represents the average spatial correlation, while the standard deviation of 0.035 reflects the uncertainty introduced by random NTD selection. These results suggest that a single model with an AUC value of less than 0.852 may not fully capture the relationships between the conditioning factors and geologic hazards. Therefore, to mitigate the random effects induced by NTDs, it is necessary to use a large number of various training datasets and calculate the AUC value of each model. Additionally, the average AUC value serves as a more reliable measure of the overall spatial relationships between the conditioning factors and geologic hazards.

3.3. Risk and return analysis

Fig. 8 presents the geologic hazard susceptibility assessment maps plotted using the four training datasets illustrated in Fig. 4. For each assessment unit, the variance

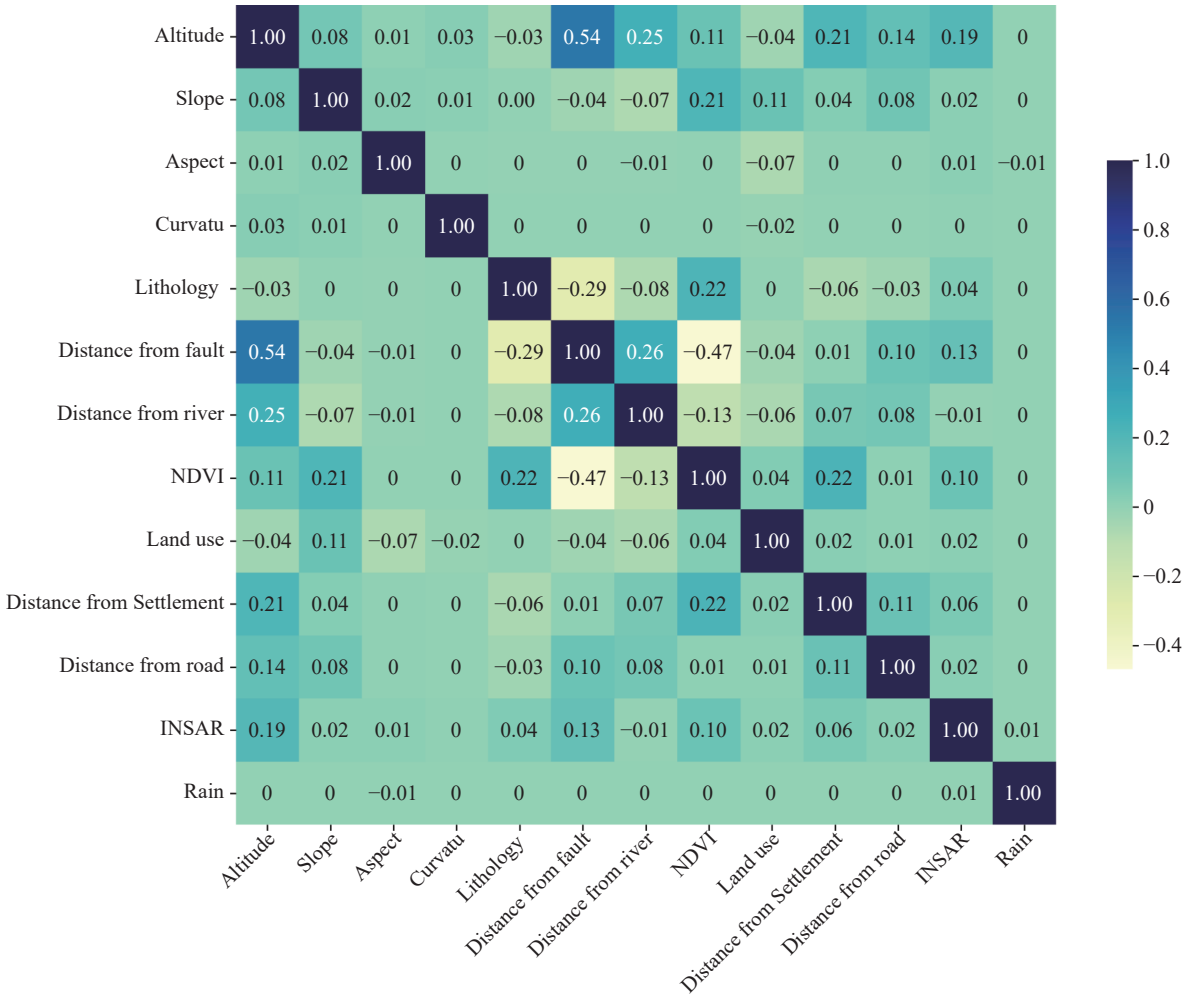

Fig. 5. Correlation matrix of conditioning factors.

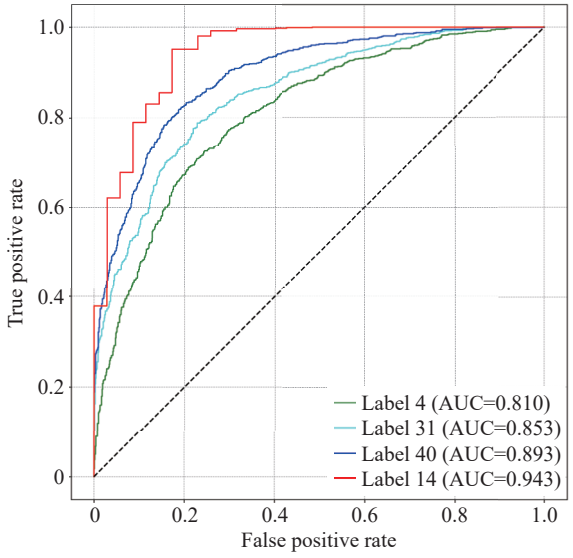

Fig. 6. ROCs of models established using four training datasets.

(Fig. 9a) and mean (Fig. 9b) of the probabilities across 40 assessment maps were calculated, representing the geologic hazard probabilities (Wang Z et al. 2020). Fig. 8 indicates that geologic hazard points are largely located in high-probability areas, exhibiting high average probability and low variance

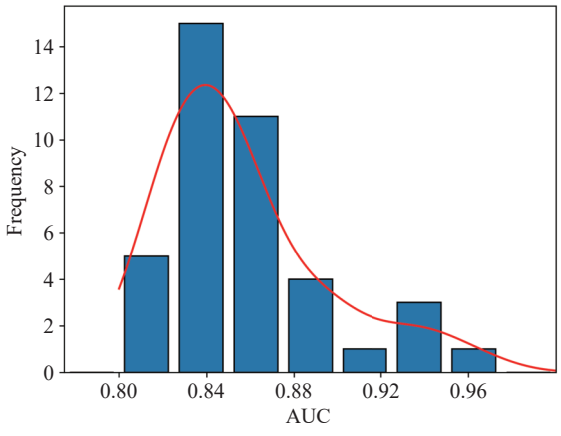

Fig. 7. Histogram of AUC values calculated based on 40 training datasets.

(Fig. 9). Additionally, this study calculated the AUC values of the variances and means, as shown in Fig. 10. According to this figure, the AUC value of the means was 0.90, indicating a strong spatial correlation between the average probability and the geologic hazard susceptibility of this region. In contrast, the AUC value of the variances was lower (0.65), reflecting a weaker spatial correlation of the variance of probability with regional geologic hazard susceptibility. These results

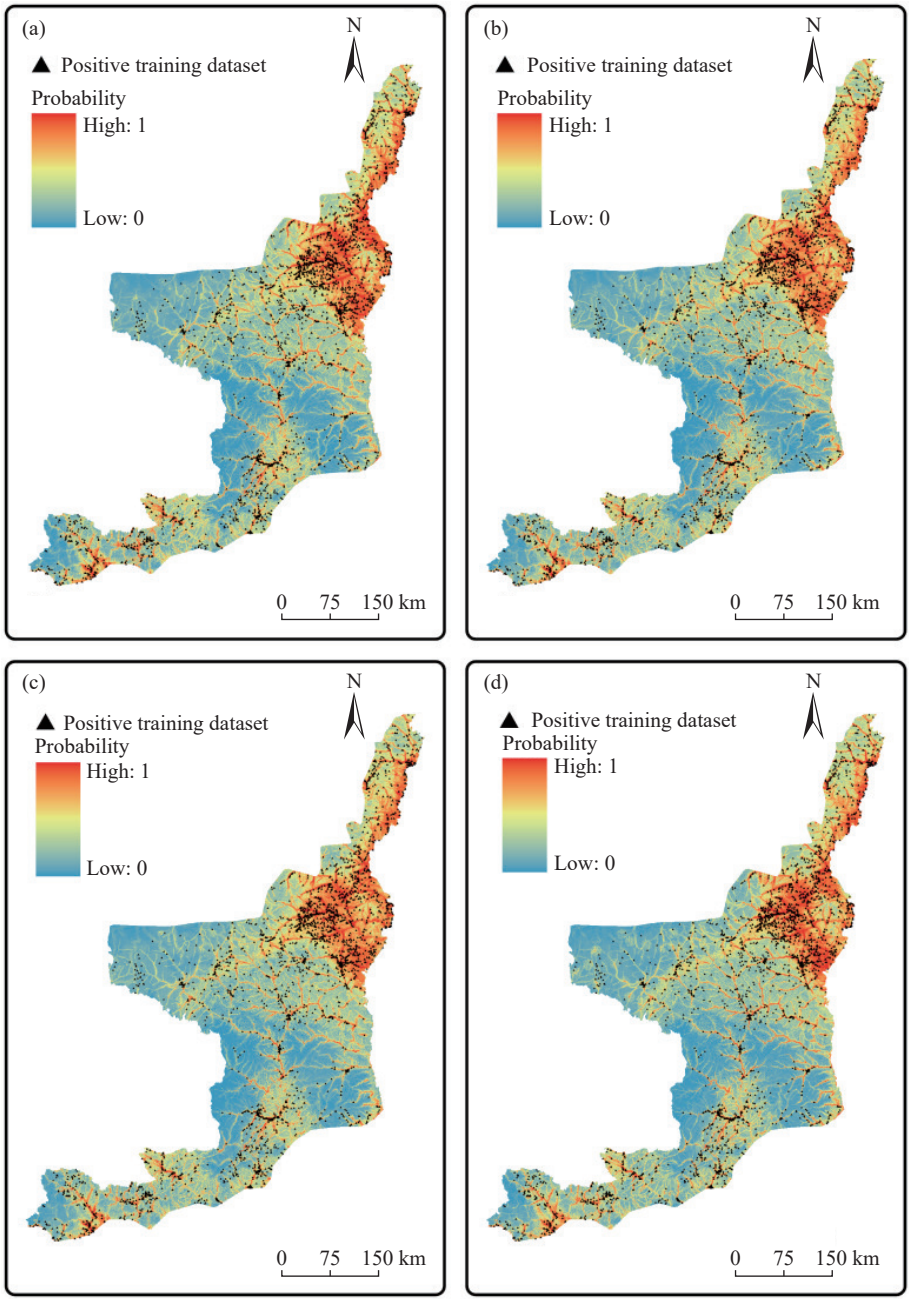

Fig. 8. Geologic hazard susceptibility assessment maps plotted using four training datasets.

demonstrate that integrating the geologic hazard probabilities of all assessment units in the 40 assessment maps can effectively generate the assessment map shown in Fig. 9b.

Using Eqs. 3 and 4, this study determined the *risk* and *return* values of the assessment units covered by all the 40 geologic hazard susceptibility assessment maps, as illustrated in Figs. 11a and b. Among these assessment units, those with lower *risk* and higher *return* values are expected to contribute greater accuracy in geologic hazard prediction. These units account for both the uncertainty introduced by the randomly selected NTDs and the high geologic hazard probabilities, thus serving as a valuable reference for plotting geologic hazard susceptibility assessment maps. In this study, the log odds ratios were converted into more intuitive probabilities, which were then used to generate a raster assessment map (Fig. 12).

4. Discussion

Compared to the geologic hazards resulting from complex geological structures, active plate movements, frequent seismic activity, and variable climatic conditions in southwestern China (Shu B et al., 2022), the geologic hazards in the Loess Plateau are primarily governed by the physical and mechanical properties of loess soils and regional tectonic stress. Notably, the unique characteristics of geologic hazards in the Loess Plateau include a high incidence of landslides and damage, which is significantly influenced by regional tectonic stress. Additionally, loess is highly sensitive to moisture, exhibiting noticeable infiltration of moving water

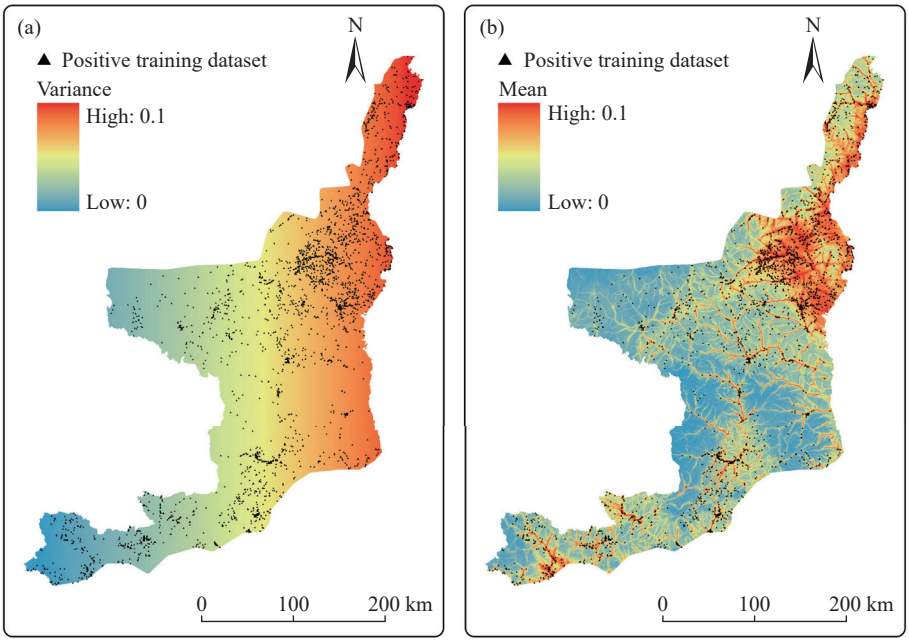

Fig. 9. Variances (a) and means (b) of 40 geologic hazard susceptibility assessment maps.

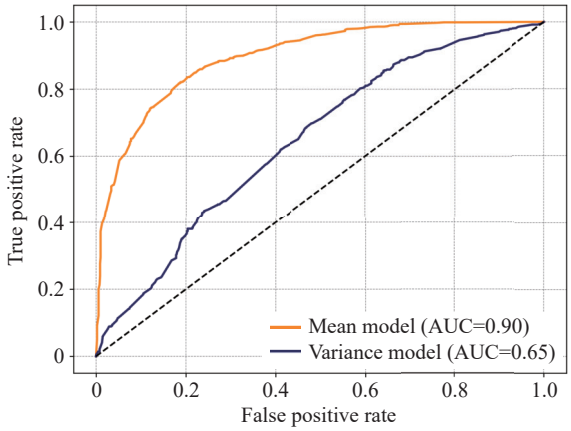

Fig. 10. ROCs of the variances (a) and means (b) of 40 geologic hazard susceptibility assessment maps.

(Peng J et al., 2020).

The loess collapses and landslides in the Loess Plateau exhibit a zonal distribution primarily due to the impact of regional tectonic stress, which serves as the main driving force behind both geologic hazard types. Loess exhibits elevated susceptibility to hazards under the combined effects of stress and moisture due to its sensitivity to water increases. This further leads to the occurrence of loess landslides and collapses. Additionally, the infiltration of surface water and groundwater is identified as a crucial external factor triggering loess collapses and landslides. Human engineering activities that alter the stress state of slopes also play a significant role in inducing geologic hazards (Sun P et al., 2022). Therefore, developing high-precision, machine learning-based geologic hazard susceptibility assessment models tailored to these unique characteristics of the Loess Plateau holds great practical significance for hazard prevention and mitigation in this region.

The dataset used in a supervised data-driven model for geologic hazard susceptibility assessment comprises both positive training datasets and randomly generated NTDs, along with various conditioning factors. However, the impacts of the NTDs on the model performance are frequently overlooked, leading to unstable model predictions (Wang Q et al. 2013). This issue has not been thoroughly examined in the context of geologic hazard susceptibility assessment (Su H et al., 2022; Yang K et al., 2024). To mitigate the model uncertainty arising from NTDs, this study employed software to randomly generate 40 NTDs. Accordingly, 40 sample datasets were built. Then, the RF algorithm was utilized to generate and analyze 40 assessment models.

Unlike previous studies, this study converted the probability value of each assessment unit into a log odds ratio in the geologic hazard susceptibility assessment, deriving the following benefits: (1) The log odds ratio was obtained by converting a probability value into a linear scale using a natural logarithmic function. This simplifies the relationship between probability and predictive variables, thus greatly facilitating analysis and modelling; (2) probability values range between 0 and 1, which can lead to numerical instability, especially when probability values approach 0 or 1. The log odds ratio mitigates the risk of underflow or overflow in numerical calculations; (3) the log odds ratio provides a more effective expression of *risk*, as it accounts for the probability of both the occurrence and non-occurrence of hazards. This is critical to geologic hazard susceptibility assessment since it offers a direct measure of potential outcomes.

This study employed the *risk* and *return* analysis in statistics to quantify and mitigate the uncertainty of model performance introduced by NTDs, with the *risk* and r*eturn* values derived using Eqs. 3 and 4. To visualize the geologic hazard susceptibility assessment maps while considering uncertainty, this study prepared a map in the form of

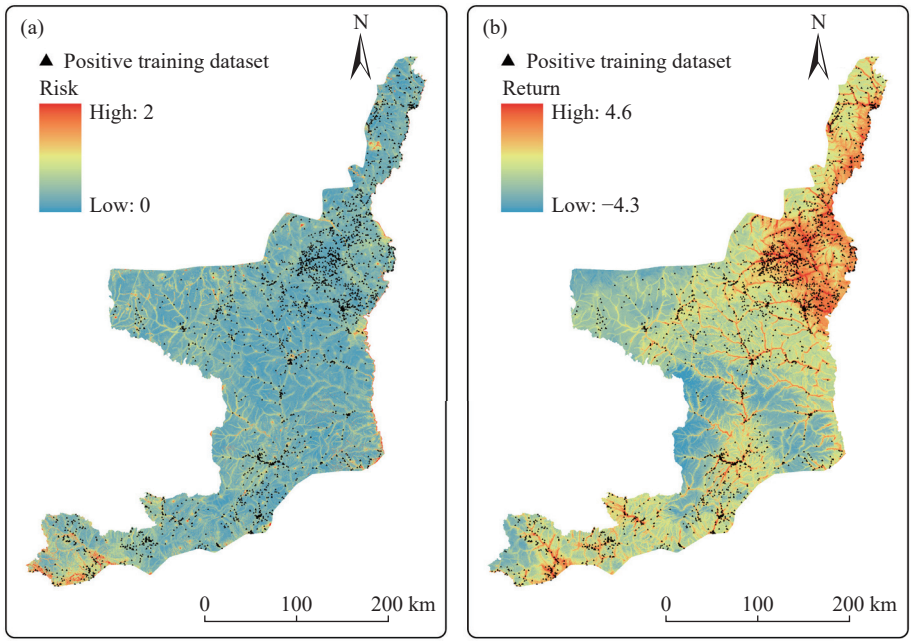

Fig. 11. Maps showing the results of *risk* (a) and *return* (b) analysis.

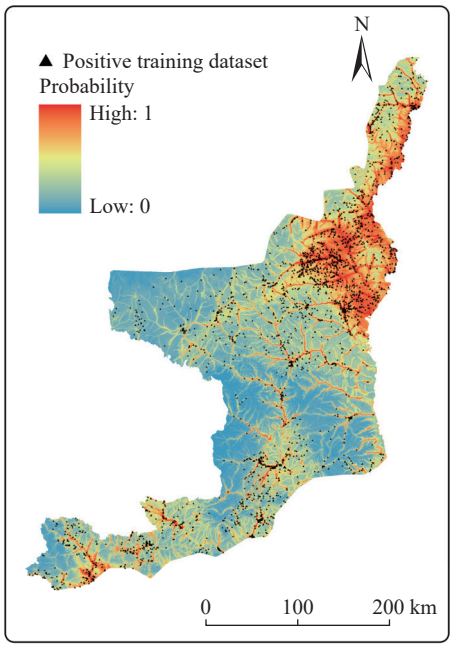

Fig. 12. Geologic hazard susceptibility assessment map generated using probabilities converted from Log odds ratios.

probability values derived from a logistic function. This map indicates that areas with high *return* values correspond to higher geologic hazard probability. To further investigate the visualization process and identify the most susceptible areas characterized by low *risk* and high *return*, the authors prepared a scatter plot consisting of the *risk* and *return* values, as shown in Fig. 13. In this plot, the *y*- and *x*-axis represent the *risk* and *return* values, respectively, and the small black triangular spots denote hazard points. This plot can be divided into four quadrants: low *risk*-low *return*, low *risk*-high *return*, high *risk*-low *return*, and high *risk*-high *return*. The geologic hazard points notably cluster in the fourth quadrant,

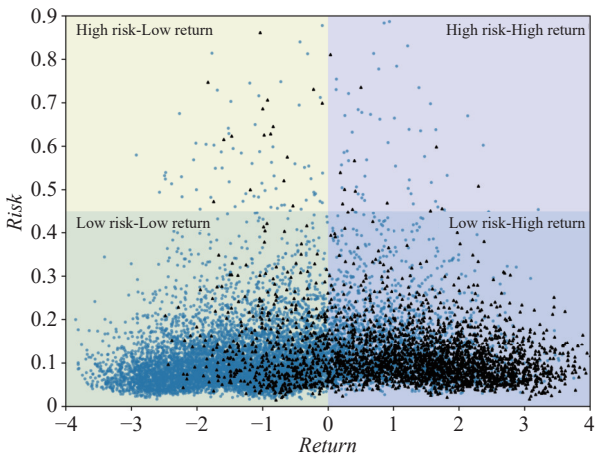

Fig. 13. *Risk* – *return* scatter plot.

corresponding to the low-*risk* and high-*return* areas. To more intuitionally present the spatial distribution characteristics of the analytical results, the authors illustrated this grouping of four quadrants in Fig. 14. According to this figure, low-*risk* and high-*return* areas exhibit a high geologic hazard susceptibility and low uncertainty. Preventive measures for these areas should be given priority. This information will assist decision-makers to effectively manage risks, formulate strategies for hazard reduction, and establish early warning systems.

5. Conclusions

This study develops an innovative framework tailored to assess the potential impacts of randomly generated NTDs on the accuracy of models for geologic hazard susceptibility assessment and to effectively quantify the uncertainty introduced by the NTDs while providing a practical solution. The integration of the RF algorithm with the *risk* and *return*

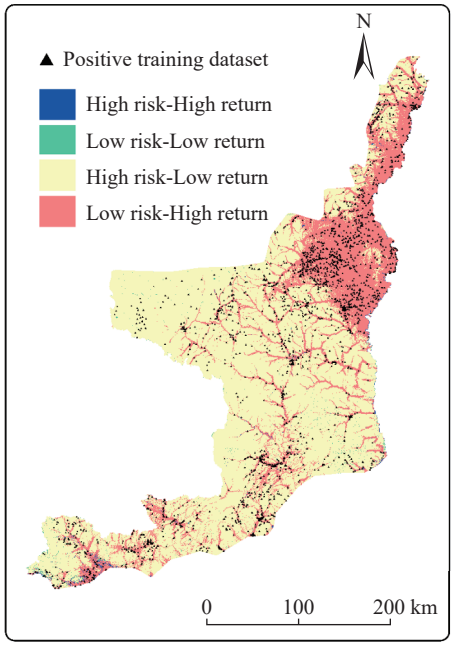

Fig. 14. Geologic hazard susceptibility map showing the spatial distributions of low *risk*-low *return*, low *risk*-high *return*, high *risk*-low *return*, and high *risk*-high *return* areas.

analysis represents a novel combination of machine learning techniques and statistical methods, offering a new perspective and tool for geologic hazard susceptibility assessment. Additionally, the introduction of the log odds ratio and its conversion into a probability value contribute to more intuitive and comprehensible assessment results, representing a methodological contribution to the field of geologic hazard susceptibility assessment. This study will significantly advance the research on geologic hazard susceptibility assessment. The findings lead to the following conclusions:

(i) This study represents the first systematical assessment of the impacts of various NTDs on models for geologic hazard susceptibility assessment. A total of 40 NTDs and 40 assessment models are used. The detailed analysis reveals that these models exhibit AUC values ranging from 0.810 to 0.963, with an average of 0.852 and a standard deviation of 0.035. These results indicate encouraging prediction effects overall and some uncertainty of these models.

(ii) The *risk* and *return* method is applied to the assessment, with the log odds ratio introduced as a probability index to measure the assessment. Log odds ratios are converted into intuitive probabilities using a logical function, improving the explanatory power and operability of the assessment results. Furthermore, such conversion allows for the effective assessment and mitigation of the uncertainty introduced by NTDs by calculating the standard deviations (*risk*) and means (*return*) of the log odds ratios of various assessment units. The predictions of low-*risk* and high-*return* areas exhibit low standard deviations and high means, indicating that the geologic hazard susceptibility assessment predictions of these areas are consistent and reliable.

(iii) The methodological framework proposed in this study has great potential for dissemination and application. This framework is suitable for geologic hazard susceptibility assessment across various regions and types, laying a solid scientific foundation for geologic hazard prevention and management. The method design, which accounts for the impacts of random NTDs, significantly enhances the generalization ability of the assessment model, allowing it to operate stably under varying geological and environmental conditions and contributing to more informed decisions regarding resource allocation and hazard management strategies.

Data availability statement

The research data of this paper can be obtained through URL https://search.asf.alaska.edu/#/ (Fig. 2a). By utilizing the relevant tools within the ArcGIS Pro software, additional terrain-related data such as curvature, slope, and aspect can be computed (Figs. 2b–d). Lithology (Fig. 2e) was provided by https://www.resdc.cn/. Data on faults (Fig. 2f) and rivers (Fig. 2g) were provided by the National Geomatics Center of China (https://www.webmap.cn/store.do?method=store&storeId=2). The NDVI values were first amplified by 10000 times from the range of –0.2–1 to –2000–10000 and were then compressed to the range of 0–255 (Liu J et al., 2005) (Fig. 2h). Land use (Fig. 2i) was provided by https://www.resdc.cn/. In the calculation of the distance from residential areas, the coordinates corresponding to these locations were obtained using the address lookup tool of mapping service software. These coordinates were then corrected using coordinate correction tools to obtain accurate coordinate information. Distance from residential areas was calculated based on these coordinates (Fig. 2j; http://www.stats.gov.cn). Distance from roads (Fig. 2k) was provided by https://www.resdc.cn/. Annual average rainfall data were obtained from the Department of Natural Resources of Shaanxi Province (https://zrzyt.shaanxi.gov.cn/; Fig. 2l). InSAR data (Fig. 2m) were accessed on the website of the European Space Agency's Sentinel dataset (https://scihub.copernicus.eu/). Then, these data were processed in the following key steps. First, image registration was performed to ensure the accurate correspondence of SAR images acquired at different times in space. Second, the interferogram was generated to reveal the deformation information of the surface during the observation period by comparing two or more SAR images. Finally, atmospheric correction was performed to eliminate the impacts of atmospheric conditions on InSAR measurements, aimed at obtaining more practical surface deformation data and providing a solid data basis for the geologic hazard susceptibility assessment.

CRediT authorship contribution statement

Hao Cheng, Wei Hong and Zhen-kai Zhan dong conceived of the presented idea. Hao Cheng, Zeng-lin Hong and Zi-yao Wang organized datasets interpretation work. Hao Cheng and Yu-xuan Dong wrote the manuscript. All authors discussed the results and contributed to the final manuscript.

Declaration of competing interest

The authors declare no conflicts of interest.

Acknowledgment

This study was supported by a project entitled *Loess Plateau Region-Watershed-Slope Geological Hazard Multi-Scale Collaborative Intelligent Early Warning System* of the National Key R&D Program of China (2022YFC3003404), a project of the Shaanxi Youth Science and Technology Star (2021KJXX-87), and public welfare geological survey projects of Shaanxi Institute of Geologic Survey (20180301, 201918, 202103, and 202413). The authors would like to extend their profound gratitude to the editors and anonymous reviewers of this manuscript for their constructive advice and corrections.

References

Abuzied SM, Mansour BMH. 2019. Geospatial hazard modeling for the delineation of flash flood-prone zones in wadi dahab basin, Egypt. Journal of Hydroinformatics, 21(1), 180–206. doi: 10.2166/hydro.2018.043.

Aida T, Silvia D. 2014. Quantitative techniques for financial risk assessment: a comparative approach using different risk measures and estimation methods. Procedia Economics and Finance, 8, 712–719. doi: 10.1016/S2212-5671(14)00149-X.

Alireza A, Biswajeet P, Luigi L. 2019. Comparative assessment using boosted regression trees, binary logistic regression, frequency ratio and numerical risk factor for gully erosion susceptibility modelling. Catena, 183 104223. doi: 10.1016/j.catena.2019.104223.

Bui DT, Tuan TA, Harald K, Biswajeet P, Inge R. 2016. Spatial prediction models for shallow landslide hazards: a comparative assessment of the efficacy of support vector machines, artificial neural networks, kernel logistic regression, and logistic model tree. Landslides, 13(2), 361–378. doi: 10.1007/s10346-015-0557-6.

Camminatiello I, D'Ambra A, Sarnacchiaro P. 2014. The association in a two-way contingency table through log odds ratio analysis: the case of sarno river pollution. Springerplus, 3(1), 384. doi: 10.1186/2193-1801-3-384.

Chang Z, Du, Zhen, Zhang F, Huang F, Chen J, Li W, Guo Z. 2020. Landslide susceptibility prediction based on remote sensing images and gis: comparisons of supervised and unsupervised machine learning models. Remote Sensing, 12(3), 502. doi: 10.3390/rs12030502.

Chang Z, Huang J, Huang F, Bhuyan K, Sansar R M, Catani F. 2023. Uncertainty analysis of non-landslide sample selection in landslide susceptibility prediction using slope unit-based machine learning models. Gondwana Research, 117 307–320. doi: 10.1016/j.gr.2023.02.00.

Chen C, Oguchi T, Hayakawa YS, Saito H, Chen H, Lin G, Wei L, Chao Y. 2018. Sediment yield during typhoon events in relation to landslides, rainfall, and catchment areas in taiwan. Geomorphology, 303 540–548. doi: 10.1016/j.geomorph.2017.11.007.

Gan Z, Yue D, Gan R, Liu X, Pei X. 2004. Characteristic on rural settlements distribution and its land use in loess hill-gully area of northern shaanxi province. Journal of Shaanxi Normal University (Natural Science Edition), 32(3), 102–106. doi: 10.3969/j.issn.1672-4291.2004.03.029.

Gao R, Wang C, Liang Z, Han S, Li B. 2021. A research on susceptibility mapping of multiple geological hazards in yanzi river basin, China. Isprs International Journal of Geo-Information, 10(4), 218. doi: 10.3390/ijgi10040218.

Gao Y, Zhang Z, Xiong Y, Zuo R. 2016. Mapping mineral prospectivity for cu polymetallic mineralization in southwest Fujian Province, China. Ore Geology Reviews, 75 16–28. doi: 10.1016/j.oregeorev.2015.12.005.

Giordan D, Luzi G, Monserrat O, and Dematteis N. 2022. Remote sensing analysis of geologic hazards. Remote Sensing, 14(19), 4818. doi: 10.3390/rs14194818.

He Y, Zhang Y. 2022. Comparison of three mixed-effects models for mass movement susceptibility mapping based on incomplete inventory in China. Remote Sensing, 14(23), 6068. doi: 10.3390/rs14236068.

Hu Y, Li Z, Wang L, Chen B, Zhu W, Zhang S, Du J, Zhang X, Yang J, Zhou M, Liu Z. 2022. Rapid interpretation and analysis of the 2022 eruption of hunga tonga-hunga ha'apai volcano with integrated remote sensing techniques. Geomatics and Information Science of Wuhan University, 47(2), 242–251. doi: 10.13203/j.whugis20220050.

Huang F, Xiong H, Zhou X, Catani F, Huang J. 2024. Modelling uncertainties and sensitivity analysis of landslide susceptibility prediction under different environmental factor connection methods and machine learning models. Ksce Journal of Civil Engineering, 28(1), 45–62. doi: 10.1007/s12205-023-2430-9.

Huang F, Ye Z, Jiang S, Huang J, Chang Z, and Chen J. 2021. Uncertainty study of landslide susceptibility prediction considering the different attribute interval numbers of environmental factors and different data-based models. Catena, 202 105250. doi: 10.1016/j.catena.2021.105250.

Kavzoglu T, Emrehan KS, Colkesen I. 2015. Selecting optimal conditioning factors in shallow translational landslide susceptibility mapping using genetic algorithm. Engineering Geology, 192 101–112. doi: 10.1016/j.enggeo.2015.04.004.

Li T, Xie C, Xu C, Qi W, Huang Y, Li L. 2024. Automated machine learning for rainfall-induced landslide hazard mapping in luhe county of Guangdong Province, China. China Geology, 7(2), 315–329. doi: 10.31035/cg2024064.

Liang SY, Wang YX, Wang Y. 2010. Risk assessment of geological hazard in wudu area of longnan city, china. Applied Mechanics and Materials, 39 232–237. doi: 10.4028/www.scientific.net/AMM.39.232.

Liu J, Liu M, Tian H, Zhuang D, Zhang Z, Zhang W, Tang X, Deng X. 2005. Spatial and temporal patterns of china's cropland during 1990–2000: an analysis based on landsat tm data. Remote Sensing of Environment, 98(4), 442–456. doi: 10.1016/j.rse.2005.08.012.

Liu L, Gao H, Li Z. 2021. Landslide susceptibility assessment based on coupling of cf model and logistic regression model in Yongjia County. Periodical of Ocean University of China, 51(10), 121–129 (in Chinese). doi: 10.16441/j.cnki.hdxb.20200247.

Liu Y, Sun H, Gong J. 2018. Geologic hazard susceptibility and disaster risk mapping based on information value model for the Mianchi County, China. Iop Conference Series. Earth and Environmental Science, 199(2), 22039. doi: 10.1088/1755-1315/199/2/022039.

Matsunaga K, Gan Z. 2007. Geological and geomorphological conditions of mass movements in the loess plateau. Bulletin of Soil and Water Conservation, 27(01), 55–57 (in Chinese). doi: 10.13961/j.cnki.stbctb.2007.01.013.

Meng Z, Ma P, Peng J. 2021. Characteristics of loess landslides triggered by different factors in the Chinese loess plateau. Journal of Mountain Science, 18(12), 3218–3229. doi: 10.1007/s11629-021-6880-6.

Merghadi A, Yunus AP, Dou J, Whiteley J, Binh T, Tien BD, Avtar R, Abderrahmane B. 2020. Machine learning methods for landslide susceptibility studies: A comparative overview of algorithm performance. Earth-Science Reviews, 207, 103225. doi: 10.1016/j.earscirev.2020.103225.

Nykanen V, Lahti I, Niiranen T, Korhonen K. 2015. Receiver operating characteristics (roc) as validation tool for prospectivity models - a magmatic ni-cu case study from the central lapland greenstone belt, northern finland. Ore Geology Reviews, 71, 853–860. doi: 10.1016/j.oregeorev.2014.09.007.

Peng J, Wang Q, Zhuang J, Leng Y, Fan Z, Wang S. 2020. Dynamic formation mechanism of landslide disaster on the loess plateau. Journal of Geomechanics, 26(5), 714–730. doi: 10.12090/j.issn.1006-6616.2020.26.05.059.

Shi Q, Wang M, Gan Z. 2007. Field survey on water erosion of the rural settlement in the loess hilly-gully area. Journal of Shaanxi Normal University (Natural Science Edition), 35(02), 103–107. doi: 10.15983/j.cnki.jsnu.2007.02.027.

Shu B, Chen Y, Amani-Beni M, Zhang R. 2022. Spatial distribution and influencing factors of mountainous geological disasters in southwest China: A fine-scale multi-type assessment. Frontiers in Environmental Science, 10, 1049333. doi: 10.3389/fenvs.2022.1049333.

Su H, Glenn F, Hu X, Wu S, Di B, Tan C. 2022. Predicting change in adaptation strategies of households to geological hazards in the longmenshan area, China using machine learning and Gis. Water, 14(7), 1023. doi: 10.3390/w14071023.

Sun P, Zhang M, Jia J, Cheng X, Zhu L, Xue Q, Wang J. 2022. Geo-hazards research and investigation in the loess regions of western China. Northwestern Geology, 55(3), 96–107 (in Chinese). doi: 10.19751/j.cnki.61-1149/p.2022.03.007.

Tazik E, Jahantab Z, Bakhtiari M, Rezaei A, Alavipanah S K. 2014. Landslide susceptibility mapping by combining the three methods fuzzy logic, frequency ratio and analytical hierarchy process in dozain basin. The International Archives of the Photogrammetry, Remote Sensing and Spatial Information Sciences, 2 (XL-2/W3), 267–272. doi: 10.5194/isprsarchives-XL-2-W3-267-2014.

Wang H, Zhang L, Yin K, Luo H, Li J. 2021. Landslide identification using machine learning. Geoscience Frontiers, 12(1), 351–364. doi: 10.1016/j.gsf.2020.02.012.

Wang Q, Guo H, Chen Y, Lin Q, Li H. 2013. Application of remote sensing for investigating mining geological hazards. International Journal of Digital Earth, 6(5), 449–468. doi: 10.1080/17538947.2011.629009.

Wang Z, Yin Z, Caers J, Zuo R. 2020. A monte carlo-based framework for risk-return analysis in mineral prospectivity mapping. Geoscience Frontiers, 11(6), 2297–2308. doi: 10.1016/j.gsf.2020.02.010.

Xu C, Ma S, Chen X. 2023. Comparison of the effects of earthquake-triggered landslide emergency hazard assessment models: A case study of the lushan earthquake with *M*w5.8 on June 1, 2022. Seismology and Geology, 45 (04), 896–913. doi: 10.3969/i.issn.0253-4967.2023.04.006.

Yang F, Wang Z, Zuo R, Sun S, Zhou B. 2023. Quantification of uncertainty associated with evidence layers in mineral prospectivity mapping using direct sampling and convolutional neural network. Natural Resources Research, 32(1), 79–98. doi: 10.1007/s11053-022-10144-6.

Yang K, Niu R, Song Y, Dong J, Zhang H, Chen J. 2024. Dynamic hazard assessment of rainfall-induced landslides using gradient boosting decision tree with google earth engine in Three Gorges reservoir area, China. Water, 16(12), 1638. doi: 10.3390/w16121638.

Yang Z, Qi W, Xu C, Shao X. 2024. Exploring deep learning for landslide mapping: A comprehensive review. China Geology, (7), 330–350. doi: 10.31035/cg2024032.

Yao J, Qin S, Qiao S, Che W, Chen Y, Su G, Miao Q. 2020. Assessment of landslide susceptibility combining deep learning with semi-supervised learning in jiaohe county, Jilin Province, China. Applied Sciences-Basel, 10(16), 5640. doi: 10.3390/app10165640.

Yhip TM, Alagheband BMD. 2020. Statistical methods of credit risk analysis. The Practice of Lending, 351–381. doi: 10.1007/978-3-030-32197-0_8.

Youssef AM, Mahdi AM, Al-Katheri MM, Pouyan S, Pourghasemi HR. 2023. Multi-hazards (landslides, floods, and gully erosion) modeling and mapping using machine learning algorithms. Journal of African Earth Sciences, 197, 104788. doi: 10.1016/j.jafrearsci.2022.104788.

Zhang H, Zeng R, Zhang Y, Zhao S, Meng X, Li Y, Liu W, Meng X, Yang Y. 2022. Subsidence monitoring and influencing factor analysis of mountain excavation and valley infilling on the Chinese loess plateau: A case study of Yan'an new district. Engineering Geology, 297, 106482. doi: 10.1016/j.enggeo.2021.106482.

Zhao Z, Chen J. 2023. A robust discretization method of factor screening for landslide susceptibility mapping using convolution neural network, random forest, and logistic regression models. International Journal of Digital Earth, 16(1), 408–429. doi: 10.1080/17538947.2023.2174192.

Zuo R, Zhang Z, Zhang D, Carranza EJM, Wang H. 2015. Evaluation of uncertainty in mineral prospectivity mapping due to missing evidence: A case study with skarn-type fe deposits in southwestern Fujian Province, China. Ore Geology Reviews, 71, 502–515. doi: 10.1016/j.oregeorev.2014.09.024.

Zuo R, Wang Z. 2020. Effects of random negative training samples on mineral prospectivity mapping. Natural Resources Research, 29(6), 3443–3455. doi: 10.1007/s11053-020-09668-6.